

Intrinsic anomalous valley Hall effect in single-layer Nb₃I₈Rui Peng, Yandong Ma,^{*} Xilong Xu, Zhonglin He, Baibiao Huang, and Ying Dai^{*}*School of Physics, State Key Laboratory of Crystal Materials, Shandong University, Shandan Street 27, Jinan 250100, China*

(Received 10 February 2020; revised 22 June 2020; accepted 24 June 2020; published 9 July 2020)

A major obstacle to reaching the wide applications of valleytronics operations is the lack of suitable anomalous valley Hall (AVH) materials, which should be easily fabricated and exhibit spontaneous valley polarization. Here, we identify an excellent two-dimensional AVH material, namely single-layer Nb₃I₈, based on first principles. Single-layer Nb₃I₈ is a robust ferromagnetic semiconductor with a moderate band gap. More importantly, due to the intrinsic breakings of both time-reversal symmetry and inversion symmetry, it exhibits the long-sought spontaneous valley polarization, without requiring any external tuning. Spontaneous valley polarization can reach as large as 107 meV, which is beneficial for practical operations. Furthermore, the experimental exfoliation of single-layer Nb₃I₈ is highly feasible as the stable layered bulk phase exists. Our findings provide an ideal platform for exploring the AVH effect and future valleytronic applications.

DOI: [10.1103/PhysRevB.102.035412](https://doi.org/10.1103/PhysRevB.102.035412)**I. INTRODUCTION**

A valley, labeling the energy extreme of a conduction or valence band, is a new degree of freedom of electrons. The existence of two or more degenerate but inequivalent valleys in the band structure leads to valley physics and potential applications in information technology. Two-dimensional (2D) materials with a hexagonal lattice provide appropriate platforms for operating valley physics when their band edges are located at the corners of the Brillouin zone ($+K$ and $-K$ points) [1–5]. Due to the large separation of $+K$ and $-K$ valleys in the momentum space, the valley index can be robust against impurity and phonon scatterings. Upon breaking inversion symmetry, the carriers at the valleys are associated with the valley contrasting physical quantities. Currently, the most studied 2D valleytronic materials are 2D transition-metal dichalcogenides (TMDs) in which inversion symmetry breaking and strong spin-orbit coupling (SOC) give rise to coupled spin and valley physics [3]. Accordingly, 2D TMDs are considered to be the most promising platform for studying the fundamental valley and spin physics. In addition to 2D TMDs, many other 2D valleytronic materials have been reported recently, including graphene [1,2], Ti₂O [6], Ti@SiC [7], and group IV or III-V binary compounds [8–11].

To use a valley index as an information carrier, it is necessary to produce valley polarization in these systems, thus realizing the anomalous valley Hall (AVH) effect. Normally, external tunings are indispensable, and several strategies have been proposed, including optical pumping [12,13], magnetic doping [14,15], the magnetic proximity effect [16–19], or a magnetic field [20,21]. As a dynamic process, optical pumping is difficult to control and thus is not suitable for information storage [12,13]. Magnetic doping suffers from the clustering effect and impurity scattering [14,15]. Magnetic

substrate usually diminishes the performance of the host material and increases energy consumption [16–19]. Finally, for a magnetic field, the efficiency is extremely low (0.2 meV/T) [20,21]. In this regard, alternative approaches are urgently needed.

Recently, the discovery of 2D “ferrovalley” materials has provided new opportunities to address these challenges. Combined with a valley index and magnetism, 2D “ferrovalley” materials possess spontaneous valley polarization without requiring any external tuning. Such materials are extremely rare, with only a few cases having been reported so far, i.e., H -VSe₂ [22,23], H -FeCl₂ [24], MnPX₃ ($X = S, Se$) [25], LaBr₂ [26], and VAgP₂Se₆ [27]. Even for these few existing systems, they suffer from many drawbacks: the experimentally observed VSe₂ is T -phase rather than H -phase, and its magnetic state is still debatable [28–30]; H -FeCl₂ is a hypothetical structure that does not exist in experiment [24]; while the valley polarizations in other systems are too small (15–43 meV) [25–27]. Therefore, for ease of experimental realization and device implementation, it is highly desirable to search for new 2D ferromagnetic semiconductors with a sizable spontaneous valley polarization.

In this work, using first-principles calculations, we propose a tantalizing 2D valleytronic semiconductor, namely single-layer (SL) Nb₃I₈. It is found that SL Nb₃I₈ is a robust ferromagnetic semiconductor with a moderate band gap. The hexagonal lattice combined with the band edges located at the $+K$ and $-K$ points renders it a promising 2D valleytronic semiconductor. More remarkably, it harbors a large spontaneous valley polarization, which reaches up to 107 meV in the conduction band, extremely favorable for further experimental characterization and practical applications. We attribute this exotic phenomenon to the combined effects of intrinsic magnetic exchange interaction and strong SOC. Under an in-plane electrical field, the rare AVH effect can readily be observed in SL Nb₃I₈ due to the valley-contrasting Berry curvature. Moreover, these phenomena proposed here exhibit a high degree of experimental feasibility as SL Nb₃I₈ can be easily

^{*}Authors to whom all correspondence should be addressed: yandong.ma@sdu.edu.cn; daiy60@sdu.edu.cn

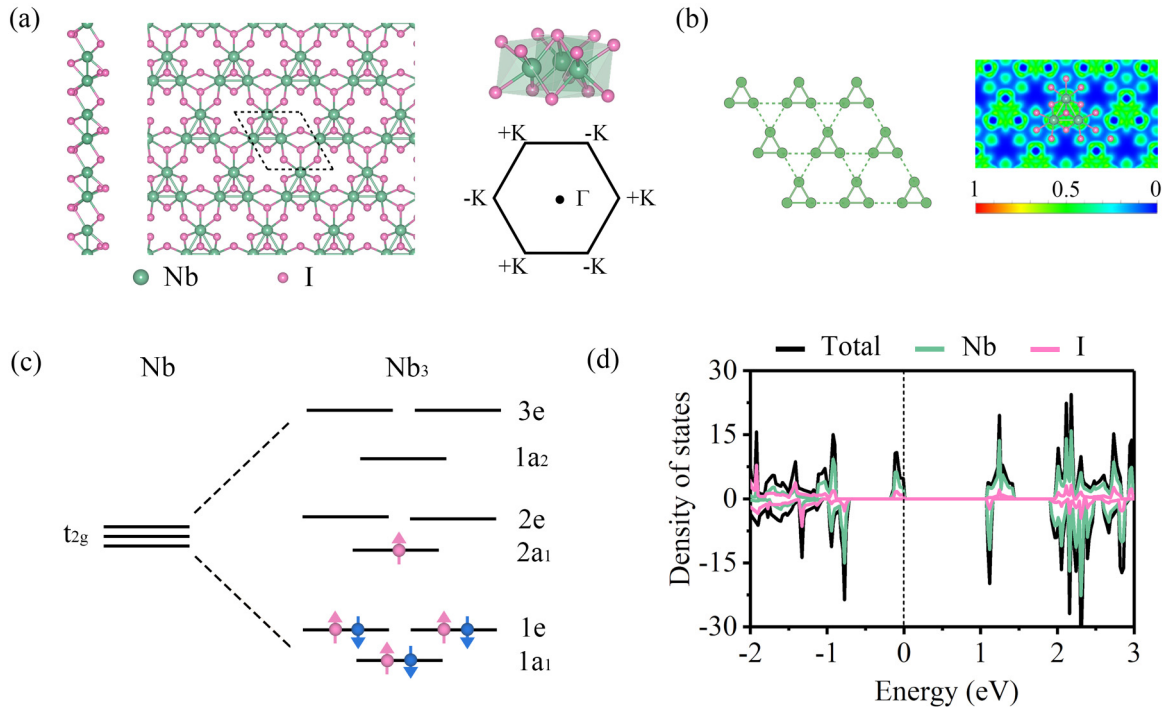


FIG. 1. (a) Crystal structure of SL Nb_3I_8 from side and top views. Insets in (a) show Nb_3I_{13} cluster unit and 2D Brillouin zone. (b) Kagome lattice formed by Nb_3 trimers and ELF of SL Nb_3I_8 . 1 and 0 in the right panel of (b) indicate accumulated and vanished electron densities, respectively. (c) d -orbital splitting of Nb_3 trimers, where red and green arrows represent spin-up and spin-down electrons, respectively. (d) Density of states of SL Nb_3I_8 .

exfoliated from the layered bulk phases. We also investigate the valleytronic properties of Nb_3Br_8 and Nb_3Cl_8 .

II. METHODS

All calculations are performed based on density functional theory [31] implemented in the Vienna Ab initio Simulation Package (VASP) [32]. The exchange-correlation interaction is treated by the generalized gradient approximation (GGA) in the form of a Perdew-Burke-Ernzerhof (PBE) functional [33]. The cutoff energy is set to 500 eV. The structures, including the lattice constant and the positions of all atoms, are relaxed until the force on each atom is less than 0.01 eV/Å. The electronic iteration convergence criterion is set to 1×10^{-5} eV. A Monkhorst-Pack (MP) grid of $5 \times 5 \times 1$ is used to sample the Brillouin zone [34]. To avoid the interaction between adjacent layers, a vacuum space of 20 Å is applied. To obtain accurate electronic structures, the HSE06 functional is employed [35]. SOC is incorporated in electronic structure calculations. For the calculations of Berry curvature and anomalous Hall conductivity, the maximally localized Wannier functions (MLWFs) implemented in the WANNIER90 package [36] are employed.

III. RESULTS

Bulk Nb_3X_8 , harboring a layered crystal structure, has been known since the 1960s [37–41]. Nb_3Cl_8 has a space group of $P-3m1$, while Nb_3Br_8 and Nb_3I_8 have a space group of $R-3m$. When Nb_3X_8 are exploited to the 2D form, they show a similar crystal structure and have a space group of $P3m1$. As

these three SL systems also share similar properties, we only focus on SL Nb_3I_8 as a representative in the following, and we discuss SL Nb_3Cl_8 and Nb_3Br_8 afterward. The lattice constant of SL Nb_3I_8 is found to be 7.64 Å. As shown in Fig. 1(a), the unit cell of SL Nb_3I_8 contains eight I atoms and three Nb atoms, with Nb atoms sandwiched between two I atomic layers. Each of the three Nb atoms assembles into a Nb_3 trimer in SL Nb_3I_8 , leading to two different Nb-Nb distances in SL Nb_3I_8 : the intratrimer distance is 3.02 Å, and the intertrimer distance is 4.63 Å. As a result, a distorted octahedral environment for Nb atom is obtained [see the inset in Fig. 1(a)]. Also, Nb trimers form a kagome lattice that contains two kinds of triangles; see Fig. 1(b). Under such a condition, inversion symmetry is broken in SL Nb_3I_8 . The electron localization function (ELF) of SL Nb_3I_8 is calculated to investigate the bonding characteristics. As shown in Fig. 1(b), the electrons are delocalized around Nb_3 trimers, indicating the formation of strong metallic bonds in the Nb_3 trimer.

Before the Nb_3X_{13} cluster forms, the d orbitals of Nb atoms split into e_g and t_{2g} . The formation of the Nb_3X_{13} cluster causes d orbitals to split into more energy levels. We can obtain $1e$, $1a_1$, $2e$, $2a_1$, $3e$, $1a_2$, which is the direct products of the t_{2g} orbitals of Nb atoms, from molecular orbital calculation; see Fig. 1(c). e , a_1 , and a_2 are irreducible representations in the C_{3v} point group, among which e is the basis function of $(d_{x^2-y^2}, d_{xy})(d_{xz}, d_{yz})$, and a_1 is the basis function of d_{z^2} . Nb atoms in each Nb_3 trimer share seven electrons, which yields a magnetic moment of $1\mu_B$. Therefore, SL Nb_3I_8 is spin-polarized. After minimizing the total energy of SL Nb_3I_8 with different spin configurations, including the nonmagnetic (NM) state, the ferromagnetic (FM) state, and

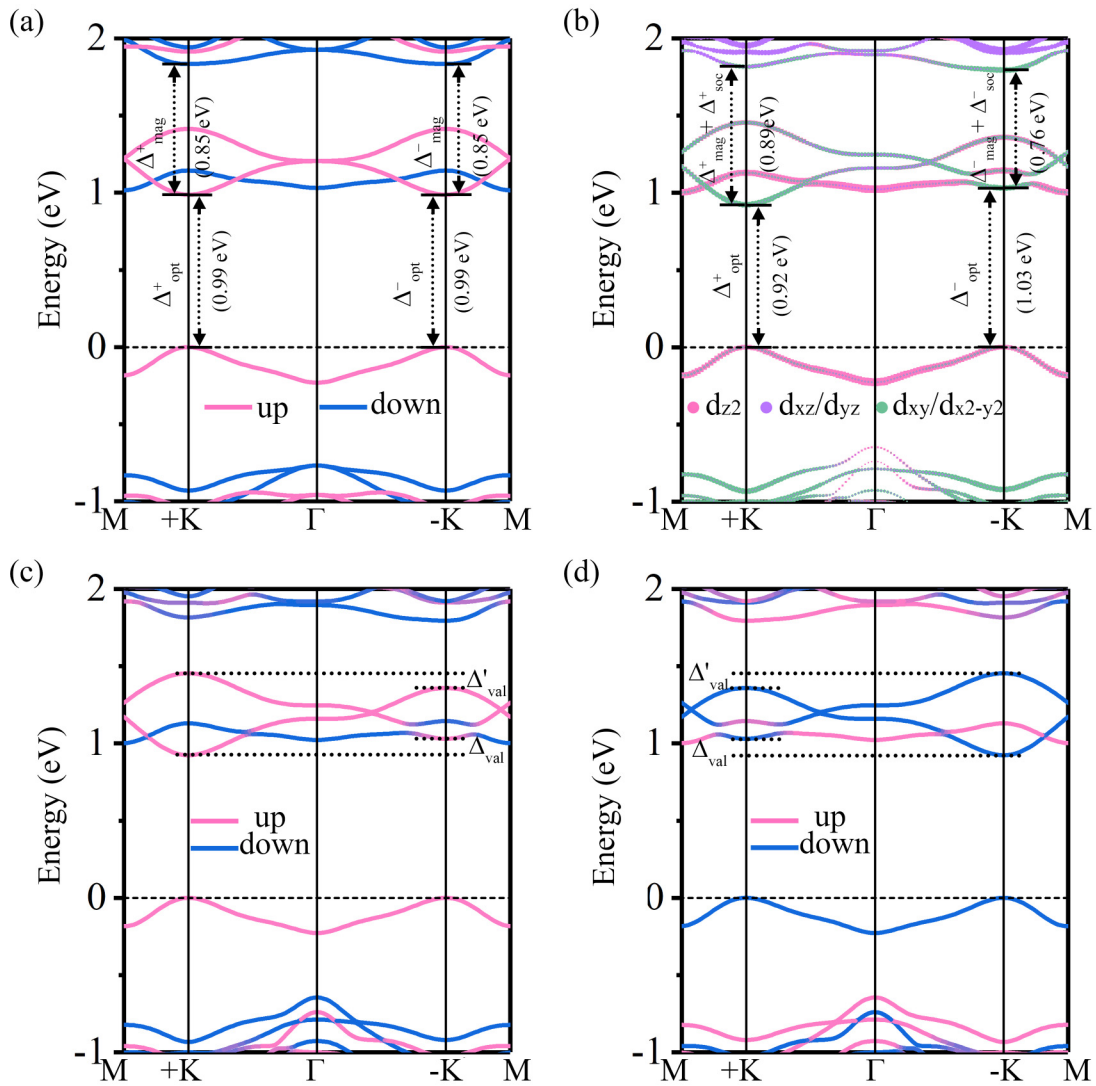


FIG. 2. (a) Spin-polarized band structure of SL Nb₃I₈ without SOC. (b) Orbital-resolved spin-polarized band structure of SL Nb₃I₈ with SOC. (c) Spin-polarized band structure of SL Nb₃I₈ with SOC. (d) The same as (c) but with opposite magnetic moment. The Fermi level is set to zero.

three kinds of antiferromagnetic (AFM) states as shown in Fig. S1 in Ref. [42], we find that the FM state exhibits the lowest energy. In detail, the FM state is 4.7, 3.3, 3.3, and 78 meV/unit cell lower than the AFM1, AFM2, AFM3, and NM states, respectively. Accordingly, the FM state is the magnetic ground state for SL Nb₃I₈, which agrees well with the previous study [43]. Although it prefers in-plane orientation, its magnetic anisotropy energy is only 0.5 meV, which can be easily manipulated by a magnetic field. In general, the magnetic moments should be localized on a single atom. However, this is not true in the case of SL Nb₃I₈, where the magnetic moments are delocalized on Nb₃ trimers. Such “cluster magnets” are robust against structural distortions and orbital couplings, which is also observed in [A]Mo₃O₈ (A represents the interstitial cations) [44,45]. The atom-resolved density of state (DOS) of SL Nb₃I₈ is shown in Fig. 1(d), from which we can see that SL Nb₃I₈ is a ferromagnetic semiconductor. The valence and conductive bands near the Fermi level

are dominated by Nb atoms, with a slight contribution from I atoms.

Figure 2(a) shows the spin-polarized band structure of SL Nb₃I₈ without SOC. It can be seen clearly that the spin-up and spin-down channels are split significantly, and the low-energy states are mainly contributed by the spin-up bands. SL Nb₃I₈ shows a direct band gap located at the corners of the 2D Brillouin zone, namely +K and -K points. In other words, the spin-up bands of SL Nb₃I₈ have one pair of valleys in both the conduction and valence bands, and the +K and -K valleys in either the conduction or valence bands are inequivalent but energetically degenerate. This suggests that SL Nb₃I₈ is a 2D valleytronic material. To manipulate the valley pseudospin in SL Nb₃I₈, breaking the balance of carriers in the inequivalent valleys is an indispensable step. To this end, external approaches are normally needed. Interestingly, when further taking SOC into account, as shown in Fig. 2(b), the valley degeneracy in SL Nb₃I₈ at the +K and -K points

is intrinsically lifted, and thus the long-sought spontaneous valley polarization is realized.

Such fantastic spontaneous valley polarization is attributed to the combined effects of magnetic exchange interaction and SOC. Without considering SOC, the magnetic exchange interaction would induce spin splitting between the spin-up and spin-down bands ($\Delta_{\text{mag}}^{\pm}$), which is the same for the $+K$ and $-K$ valleys ($\Delta_{\text{mag}}^+ = \Delta_{\text{mag}}^-$). When excluding magnetic exchange interaction, SOC would also generate spin splitting at both the $+K$ and $-K$ valleys ($\Delta_{\text{soc}}^{\pm}$). But different from $\Delta_{\text{mag}}^{\pm}$, $\Delta_{\text{soc}}^{\pm}$ is valley-dependent, with valley index $\tau = \pm 1$ for the $\pm K$ point. That is to say, the spin splitting induced by SOC alone would result in $+K$ and $-K$ valleys with opposite spin signs, but still being energetically degenerate ($\Delta_{\text{soc}}^+ = -\Delta_{\text{soc}}^-$). Accordingly, the combined effects of magnetic exchange interaction and SOC give rise to an overall spin splitting of $\Delta_{\text{mag}}^+ + \Delta_{\text{soc}}^+$ at the $+K$ point, while it is $\Delta_{\text{mag}}^- + \Delta_{\text{soc}}^-$ at the $-K$ point, yielding a valley polarization spontaneously. This scenario is quite different from other 2D valleytronic systems, such as graphene [1,2] and TMDs [3]. In these systems, due to the protection of time-reversal symmetry, the magnetic exchange interaction induced spin splitting $\Delta_{\text{mag}}^{\pm}$ is absent, and the overall spin splitting is only induced by SOC. In this regard, the two valleys will be energetically degenerate, only with opposite spin signs, and thus complicated external methods are required to produce valley polarization in these systems [1–3].

To characterize the spontaneous valley polarization in SL Nb₃I₈, we define Δ_{val}^c (Δ_{val}^v) as the energy difference between the $-K$ and $+K$ valleys in the conduction band (valence band). As shown in Fig. 2(c), the valley polarization in the conduction bands is up to 107 meV, much larger than those in LaBr₂ (33 meV) [26], MnPX₃ (43 meV) [25], VAgP₂Se₆ (15 meV) [27], and some modulated systems like WS₂/MnO₂ [19] (43 meV) and Cr/V-doped MoSSe (10–60 meV) [15]. This giant value is equivalent to the case in which a valley degenerate system is under a magnetic field of 618 T, and is robust against the external perturbations. It should be noted that although SL FeCl₂ exhibits a comparable valley polarization, it is a hypothetical structure that does not exist in experiment [24]. When the magnetic moment in SL Nb₃I₈ is reversed, as displayed in Fig. 2(d), Δ_{val}^c is reversed to -107 meV. Similar to ferromagnetism, such materials with spontaneous valley polarization are termed a ‘‘ferrovalley.’’

In contrast to the giant valley polarization in the conduction bands, the $+K$ and $-K$ valleys in the valence bands are almost degenerate, with a small valley polarization of -0.67 meV; see Fig. 2(c). To get insight into this discrepancy, we analyze the orbitals’ contribution of the band edges of SL Nb₃I₈. Figure S2 in Ref. [42] shows the atom-resolved band structure and DOS of SL Nb₃I₈, from which we can see that the conduction and valence bands near the Fermi level are mainly contributed by Nb atoms, and the contributions from I atoms lie far away from the Fermi level. More specifically, as shown in Fig. 2(b), the lowest conduction band is dominated by Nb- d_{xy/x^2-y^2} orbitals, while the highest valence band is mainly from d_{z^2} orbitals. As we mentioned above, SOC plays an important role for valley polarization in magnetic systems. The SOC Hamiltonian \hat{H}^0 represents interaction between the same spin states, and \hat{H}^1 represents interaction between

opposite spin states. They can be expressed as the following forms [46,47]:

$$\begin{aligned}\hat{H}^0 &= \lambda \hat{S}_z \left(\hat{L}_z \cos \theta + \frac{1}{2} \hat{L}_+ e^{-i\phi} \sin \theta + \frac{1}{2} \hat{L}_- e^{+i\phi} \sin \theta \right), \\ \hat{H}^1 &= \frac{\lambda}{2} (\hat{S}_+ + \hat{S}_-) \\ &\quad \times \left(-\hat{L}_z \sin \theta + \frac{1}{2} \hat{L}_+ e^{-i\phi} \cos \theta + \frac{1}{2} \hat{L}_- e^{+i\phi} \cos \theta \right),\end{aligned}$$

where \hat{L} and \hat{S} represent the orbital angular moment and spin angular moment, respectively. (x, y, z) and (x', y', z') are coordinates for \hat{L} and \hat{S} , respectively. θ and ϕ are polar angles defining the spin orientations as depicted in Fig. S2. $\hat{L}_+ = \hat{L}_x + i\hat{L}_y$, $\hat{L}_- = \hat{L}_x - i\hat{L}_y$, $\hat{S}_+ = \hat{S}_x + i\hat{S}_y$, and $\hat{S}_- = \hat{S}_x - i\hat{S}_y$. Here, we ignore the interaction between opposite spin states (\hat{H}^1) because spin degeneracy between the spin-up and spin-down bands is significantly broken in SL Nb₃I₈. In addition, as the magnetocrystalline direction in SL Nb₃I₈ is out-of-plane ($\theta = 0$), \hat{H}^0 can be simplified as $\hat{H}^0 = \lambda \hat{S}_z \hat{L}_z = \alpha \hat{L}_z$. As the group symmetry of the $+K/-K$ point is C_{3v} , the adapted basis functions are chosen as the following forms:

$$\begin{aligned}|\varphi_c^\tau\rangle &= \sqrt{\frac{1}{2}} (|d_{x^2-y^2}\rangle + i\tau |d_{xy}\rangle), \\ |\varphi_v\rangle &= |d_{z^2}\rangle,\end{aligned}$$

where c and v represent conduction and valence bands, and τ indicates the valley index. It should be noted that because the three Nb atoms in a unit cell share seven electrons together and are connected by metal bonds, we regard them as one atom and we represent the basis function by $|\varphi_c^\tau\rangle$. Finally, we obtain the energy levels of the valleys:

$$\begin{aligned}E_c^\tau &= \langle \varphi_c^\tau | \hat{H}^0 | \varphi_c^\tau \rangle \\ &= \frac{1}{2} (\langle d_{x^2-y^2} | \hat{H}^0 | d_{x^2-y^2} \rangle + \tau^2 \langle d_{xy} | \hat{H}^0 | d_{xy} \rangle) \\ &\quad + (i\tau \langle d_{x^2-y^2} | \hat{H}^0 | d_{xy} \rangle - i\tau \langle d_{xy} | \hat{H}^0 | d_{x^2-y^2} \rangle), \\ E_v^\tau &= \langle \varphi_v | \hat{H}^0 | \varphi_v \rangle = \langle d_{z^2} | \hat{H}^0 | d_{z^2} \rangle.\end{aligned}$$

Therefore, we can easily understand the discrepancy of the valley polarizations in the conduction and valence bands of SL Nb₃I₈ through

$$\begin{aligned}\Delta_{\text{val}}^c &= E_c^- - E_c^+ = i \langle d_{xy} | \hat{H}^0 | d_{x^2-y^2} \rangle - i \langle d_{x^2-y^2} | \hat{H}^0 | d_{xy} \rangle \\ &= -4\alpha, \\ \Delta_{\text{val}}^v &= E_v^- - E_v^+ = 0, \\ \Delta_{\text{val}}^v &= E_v^- - E_v^+ = 0,\end{aligned}$$

where we have used $\hat{L}_z |d_{x^2-y^2}\rangle = 2i |d_{xy}\rangle$, $\hat{L}_z |d_{xy}\rangle = -2i |d_{x^2-y^2}\rangle$.

In addition to the two pairs of valleys discussed above, as shown in Fig. 2(c), there is another pair of valleys in the second-lowest conduction band of the spin-up channel. These two valleys are mainly contributed by Nb- $d_{x^2-y^2}$, d_{xy} , and d_{z^2} orbitals. The valley polarization in the second-lowest conduction band, defined as Δ'_{val} , is found to be -95 meV, which is a little smaller than that of the lowest conduction band, but is still sizable. Two pairs of valleys such as these

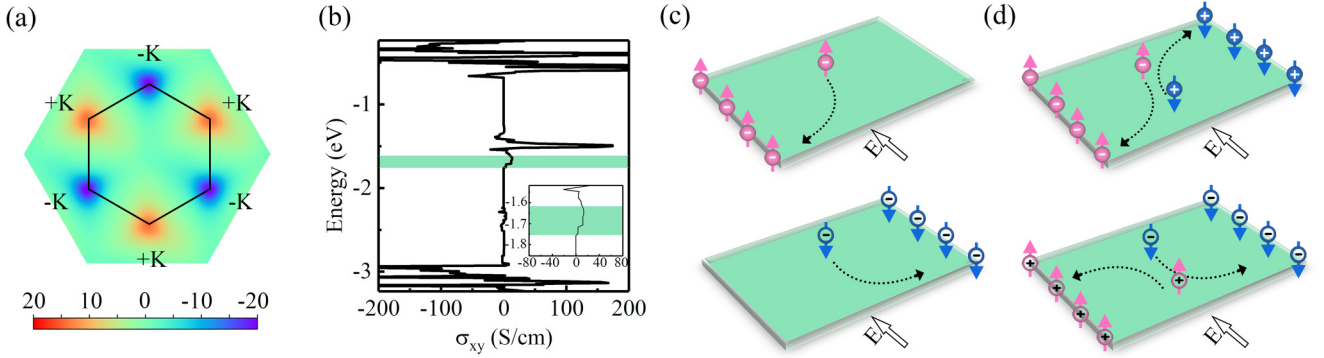


FIG. 3. (a) Contour map of Berry curvature of SL Nb₃I₈ over the entire 2D Brillouin zone. (b) Anomalous Hall conductivity of SL Nb₃I₈. The shaded region in (b) denotes the energy levels of the two valleys in the lowest conduction band and is zoomed in. Diagrams of the AVH effect under (c) electron doping and (d) light irradiation. The “+” and “-” symbols represent electrons and holes, the dark and hollow circles represent +K and -K valleys, and the red and green arrows in (c,d) represent spin-up and spin-down states, respectively.

in the conduction band have rarely been reported in previous works. Another interesting point we wish to address is that although Nb trimers in SL Nb₃I₈ form a kagome lattice [see Fig. 1(b)], the typical kagome bands are not observed here [48,49]. The absence of typical kagome bands originates from the strong metallic bonds in the Nb₃ trimer. When the intratrimer coupling is much larger than the intertrimer coupling, such kinds of bands are expected.

It is known that in systems with broken inversion symmetry, the carriers in the +K and -K valleys will acquire a nonzero Berry curvature Ω along the out-of-plane direction, giving rise to interesting valley-contrasting physics. When further breaking time-reversal symmetry, the valley-contrasting physics will be preserved, and intriguing valley-dependent phenomena such as the VAH effect will be observed. To confirm this, we calculate the Berry curvature Ω on the basis of the Kudo formula, which can be written as [50]

$$\Omega(k) = - \sum_n \sum_{n' \neq n} f_n \frac{2Im\langle \psi_{nk} | v_x | \psi_{n'k} \rangle \langle \psi_{n'k} | v_y | \psi_{nk} \rangle}{(E_n - E_{n'})^2}.$$

Here, f_n is the Fermi-Dirac distribution function, ψ_{nk} is the Bloch wave function with eigenvalue E_n , and $v_{x/y}$ is the velocity operator along the x/y direction. As shown in Fig. 3(a) and Fig. S3 in Ref. [42], the Berry curvatures of SL Nb₃I₈ at the +K and -K points have different absolute values with opposite signs, suggesting the valley-contrasting characteristic.

Under an in-plane electric field E , Bloch electrons in SL Nb₃I₈ will acquire an anomalous velocity $v \sim E \times \Omega(k)$. As signs of Berry curvature are opposite, the electrons in the +K and -K valleys will move to opposite edges of SL Nb₃I₈. When shifting the Fermi level between the +K and -K valleys in the conduction band, as shown in Fig. 3(c), the spin-up electrons in SL Nb₃I₈ from the +K valley are accumulated at the left edge of the sample under an in-plane electric field, thus realizing the AVH effect. Upon reversing SL Nb₃I₈ with opposite magnetic moment, the absolute values of Berry curvature at the +K and -K valleys will be exchanged, while their signs will stay the same. In this case, the spin-down electrons from the -K valley are accumulated at the right edge of the sample under an in-plane electric field.

As electrons are only accumulated at one edge of the sample, a more easily measurable charge Hall current as a voltage can be detected, offering a possible avenue to realize data storage using valley polarization. To confirm this, we calculate the anomalous Hall conductivity σ using the following equation [51]:

$$\sigma = - \frac{e^2}{\hbar} \int \frac{d^2k}{(2\pi)^2} \Omega(k).$$

As shown in Fig. 3(b), when the Fermi level is shifted between the +K and -K valleys in the conduction band, a fully valley-polarized Hall conductivity will be generated (marked by the shaded region). Therefore, based on the AVH effect, we can detect the valley pseudospin in SL Nb₃I₈ by direct electric measurement.

In addition to Berry curvature Ω , another valley-contrasting quantity is the orbital magnetic moment m , which is accompanied by a valley-dependent selection rule for optical excitation. Normally, to realize the AVH with optical excitation, circularly polarized light is required. Interestingly, in SL Nb₃I₈, even linearly polarized light has valley-dependent selection. When the frequency of the incident light ω meeting the requirement of $\Delta_{\text{opt}}^+ \leq \omega \hbar \leq \Delta_{\text{opt}}^-$, the spin-up electrons and spin-down holes at the +K valley will be generated. Under the in-plane electric field, the photogenerated electrons and holes will move toward opposite directions, achieving the AVH effect; see Fig. 3(d). Similar phenomena can also be observed when the magnetic moment is reversed in SL Nb₃I₈.

Having explored the valley-dependent physics of SL Nb₃I₈, we now turn to the modulation of its valley polarization. The external magnetic field, which can engineer the spin orientation, is expected to be an effective approach to control the valley polarization of SL Nb₃I₈. As shown in Figs. 4(a) and 4(b), the valley polarization of SL Nb₃I₈ is sensitive to spin orientation. When the spin orientation is along the in-plane direction ($\theta = 90^\circ$), the valley polarization of SL Nb₃I₈ vanishes. When the spin orientation is reversed ($\theta = 180^\circ$), the valley polarization of SL Nb₃I₈ is also reversed. In addition, since the orbital interaction is closely related to lattice constants, in-plane strain can also be utilized to engineer valley polarization. As shown in Figs. 4(c) and 4(d), by exerting in-plane biaxial strain from -3% to 3%, the valley

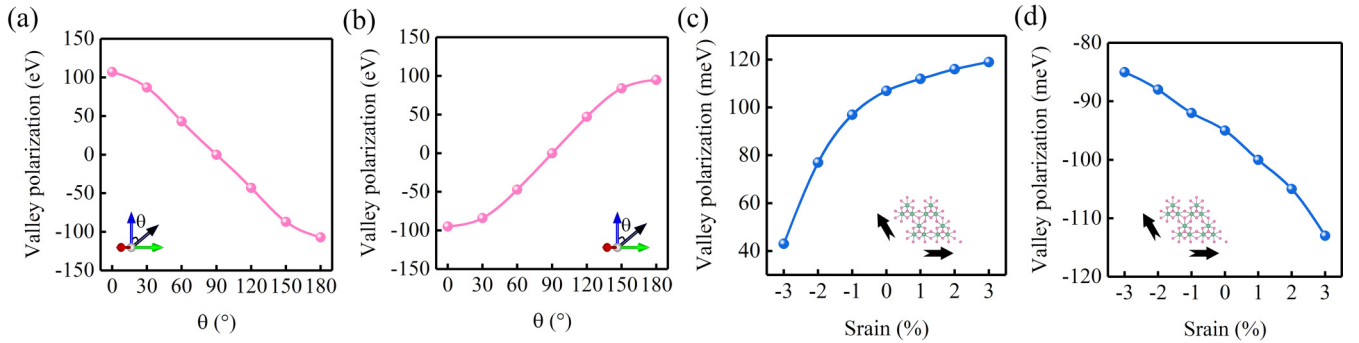


FIG. 4. Valley polarizations (a) Δ_{val}^c and (b) $\Delta_{\text{val}}^{c'}$ of SL Nb₃I₈ as a function of spin orientation. Valley polarizations (c) Δ_{val}^c and (d) $\Delta_{\text{val}}^{c'}$ of SL Nb₃I₈ as a function of in-plane strain.

polarization Δ_{val}^c ($\Delta_{\text{val}}^{c'}$) of SL Nb₃I₈ increases from 43 (–85) meV to 119 (–113) meV.

Finally, we discuss the related properties of SL Nb₃Br₈ and Nb₃Cl₈. Their band structures are shown in Fig. S4 in Ref. [42]. It can be seen that the spin-up states of SL Nb₃Br₈ have a direct band gap. Upon introducing SOC, a large valley polarization of 111 meV appears spontaneously in the conduction band of spin-up states. However, the electrical valley Hall effect seems difficult to apply straightforwardly due to the spin-down band located in the gap of the spin-up states, while for SL Nb₃Cl₈ the spin-up states have an indirect band gap, with the CBM located at the $\pm K$ point and the VBM located at the Γ point. The indirect-band-gap characteristic and the spin-down band located in the gap of the spin-up states make SL Nb₃Cl₈ also less suitable for valleytronics. Therefore, SL Nb₃I₈ is a much better choice for valleytronic application.

IV. CONCLUSION

To summarize, through first-principles calculations we reveal the intriguing spontaneous valley polarization in SL Nb₃X₈, among which SL Nb₃I₈ is an extraordinary 2D valleytronic material with intrinsic valley polarization, with-

out requiring any external modulations. The spontaneous valley polarization in SL Nb₃I₈ is as large as 107 meV, beneficial for practical applications. This fascinating phenomenon can be attributed to the combined effects of intrinsic magnetic exchange interaction and strong SOC, superior to the valley polarizations induced by external methods. Considering the experimental feasibility of these systems, the AVH effect in SL Nb₃I₈ exhibits a high experimental feasibility. Our work offers an ideal platform for exploring AVH effect and the potential applications.

ACKNOWLEDGMENTS

This work is supported by the National Natural Science Foundation of China (No. 11804190), Shandong Provincial Natural Science Foundation of China (No. ZR2019QA011 and No. ZR2019MEM013), Shandong Provincial Key Research and Development Program (Major Scientific and Technological Innovation Project) (No. 2019JZZY010302), Shandong Provincial Key Research and Development Program (No. 2019RKE27004), Qilu Young Scholar Program of Shandong University, and Taishan Scholar Program of Shandong Province.

- [1] D. Xiao, W. Yao, and Q. Niu, Valley-Contrasting Physics in Graphene: Magnetic Moment and Topological Transport, *Phys. Rev. Lett.* **99**, 236809 (2007).
- [2] W. Yao, D. Xiao, and Q. Niu, Valley-dependent optoelectronics from inversion symmetry breaking, *Phys. Rev. B* **77**, 235406 (2008).
- [3] D. Xiao, G.-B. Liu, W. Feng, X. Xu, and W. Yao, Coupled Spin and Valley Physics in Monolayers of MoS₂ and Other Group-VI Dichalcogenides, *Phys. Rev. Lett.* **108**, 196802 (2012).
- [4] X. Xu, W. Yao, D. Xiao, and T. F. Heinz, Spin and pseudospins in layered transition metal dichalcogenides, *Nat. Phys.* **10**, 343 (2014).
- [5] J. R. Schaibley, H. Yu, G. Clark, P. Rivera, J. S. Ross, K. L. Seyler, W. Yao, and X. Xu, Valleytronics in 2D materials, *Nat. Rev. Mater.* **1**, 16055 (2016).
- [6] Y. Ma, L. Kou, A. Du, B. Huang, Y. Dai, and T. Heine, Conduction-band valley spin splitting in single-layer H-Tl₂O, *Phys. Rev. B* **97**, 035444 (2018).
- [7] Z. Xu, Q. Zhang, Q. Shen, Y. Cheng, U. Schwingenschlöggl, and W. Huang, First-principles prediction of TI/SiC for valleytronics, *J. Mater. Chem. C* **5**, 10427 (2017).
- [8] D. Di Sante, A. Stroppa, P. Barone, M.-H. Whangbo, and S. Picozzi, Emergence of ferroelectricity and spin-valley properties in two-dimensional honeycomb binary compounds, *Phys. Rev. B* **91**, 161401 (2015).
- [9] T. Zhou, J. Zhang, B. Zhao, H. Zhang, and Z. Yang, Quantum spin-quantum anomalous Hall insulators and topological transitions in functionalized Sb(111) monolayers, *Nano Lett.* **15**, 5149 (2015).
- [10] S. Cheng, R. Zhang, J. Zhou, H. Jiang, and Q.-F. Sun, Perfect valley filter based on a topological phase in a disordered Sb monolayer heterostructure, *Phys. Rev. B* **97**, 085420 (2018).
- [11] M. Ezawa, Spin valleytronics in silicene: Quantum spin Hall-quantum anomalous Hall insulators and single-valley semimetals, *Phys. Rev. B* **87**, 155415 (2013).

- [12] K. F. Mak, K. He, J. Shan, and T. F. Heinz, Control of valley polarization in monolayer MoS₂ by optical helicity, *Nat. Nanotech.* **7**, 494 (2012).
- [13] H. Zeng, J. Dai, W. Yao, D. Xiao, and X. Cui, Valley polarization in MoS₂ monolayers by optical pumping, *Nat. Nanotech.* **7**, 490 (2012).
- [14] X. Xu, Y. Ma, T. Zhang, C. Lei, B. Huang, and Y. Dai, Nonmetal-atom-doping-induced valley polarization in single-layer Ti₂O, *J. Phys. Chem. Lett.* **10**, 4535 (2019).
- [15] R. Peng, Y. Ma, S. Zhang, B. Huang, and Y. Dai, Valley polarization in Janus single-layer MoSSe via magnetic doping, *J. Phys. Chem. Lett.* **9**, 3612 (2018).
- [16] C. Ke, Y. Wu, W. Yang, Z. Wu, C. Zhang, X. Li, and J. Kang, Large and controllable spin-valley splitting in two-dimensional WS₂/h - VN heterostructure, *Phys. Rev. B* **100**, 195435 (2019).
- [17] J. Qi, X. Li, Q. Niu, and J. Feng, Giant and tunable valley degeneracy splitting in MoTe₂, *Phys. Rev. B* **92**, 121403 (2015).
- [18] L. Xu, M. Yang, L. Shen, J. Zhou, T. Zhu, and Y. P. Feng, Large valley splitting in monolayer WS₂ by proximity coupling to an insulating antiferromagnetic substrate, *Phys. Rev. B* **97**, 041405 (2018).
- [19] B. Zhou, Z. Li, J. Wang, X. Niu, and C. Luan, Tunable valley splitting and an anomalous valley Hall effect in hole-doped WS₂ by proximity coupling with a ferromagnetic MnO₂ monolayer, *Nanoscale* **11**, 13567 (2019).
- [20] G. Aivazian, Z. Gong, A.M. Jones, R.-L. Chu, J. Yan, D. G. Mandrus, C. Zhang, D. Cobden, W. Yao, and X. Xu, Magnetic control of valley pseudospin in monolayer WSe₂, *Nat. Phys.* **11**, 148 (2015).
- [21] X.-X. Zhang, T. Cao, Z. Lu, Y.-C. Lin, F. Zhang, Y. Wang, Z. Li, J. C. Hone, J. A. Robinson, D. Smirnov, S. G. Louie, and T. F. Heinz, Magnetic brightening and control of dark excitons in monolayer WSe₂, *Nat. Nanotech.* **12**, 883 (2017).
- [22] W.-Y. Tong, S.-J. Gong, X. Wan, and C.-G. Duan, Concepts of ferrovalley material and anomalous valley Hall effect, *Nat. Commun.* **7**, 13612 (2016).
- [23] J. Liu, W.-J. Hou, C. Cheng, H.-X. Fu, J.-T. Sun, and S. Meng, Intrinsic valley polarization of magnetic VSe₂ monolayers, *J. Phys.: Condens. Matter* **29**, 255501 (2017).
- [24] P. Zhao, Y. Ma, H. Wang, B. Huang, L. Kou, and Y. Dai, Intrinsic valley polarization and anomalous valley Hall effect in single-layer 2H-FeCl₂, [arXiv:2003.04561](https://arxiv.org/abs/2003.04561).
- [25] X. Li, T. Cao, Q. Niu, J. Shi, and J. Feng, Coupling the valley degree of freedom to antiferromagnetic order, *Proc. Natl. Acad. Sci. (USA)* **110**, 3738 (2013).
- [26] P. Zhao, Y. Ma, C. Lei, H. Wang, B. Huang, and Y. Dai, Single-layer LaBr: Two-dimensional valleytronic semiconductor with spontaneous spin and valley polarizations, *Appl. Phys. Lett.* **115**, 261605 (2019).
- [27] Z. Song, X. Sun, J. Zheng, F. Pan, Y. Hou, M.-H. Yung, J. Yang, and J. Lu, Spontaneous valley splitting and valley pseudospin field effect transistors of monolayer VAgP₂Se₆, *Nanoscale* **10**, 13986 (2018).
- [28] W. Zhao, B. Dong, Z. Guo, G. Su, R. Gao, W. Wang, and L. Cao, Colloidal synthesis of VSe₂ single-layer nanosheets as novel electrocatalysts for the hydrogen evolution reaction, *Chem. Commun.* **52**, 9228 (2016).
- [29] P. M. Coelho, K. Nguyen Cong, M. Bonilla, S. Kolekar, M.-H. Phan, J. Avila, M. C. Asensio, I. I. Oleynik, and M. Batzill, Charge density wave state suppresses ferromagnetic ordering in VSe₂ monolayers, *J. Phys. Chem. C* **123**, 14089 (2019).
- [30] J. Feng, D. Biswas, A. Rajan, M. D. Watson, F. Mazzola, O. J. Clark, K. Underwood, I. Marković, M. McLaren, A. Hunter, D. M. Burn, L. B. Duffy, S. Barua, G. Balakrishnan, F. Bertran, P. Le Fèvre, T. K. Kim, G. van der Laan, T. Hesjedal, P. Wahl, and P. D. C. King, Electronic structure and enhanced charge-density wave order of monolayer VSe₂, *Nano Lett.* **18**, 4493 (2018).
- [31] W. Kohn and L. J. Sham, Self-consistent equations including exchange and correlation effects, *Phys. Rev.* **140**, A1133 (1965).
- [32] J. Kresse and J. Furthmüller, Efficient iterative schemes for *ab initio* total-energy calculations using a plane-wave basis set, *Phys. Rev. B* **54**, 11169 (1996).
- [33] J. P. Perdew, K. Burke, and M. Ernzerhof, Generalized Gradient Approximation Made Simple, *Phys. Rev. Lett.* **77**, 3865 (1996).
- [34] H. J. Monkhorst and J. D. Pack, Special points for Brillouin-zone integrations, *Phys. Rev. B* **13**, 5188 (1976).
- [35] J. Heyd, G. E. Scuseria, and M. Ernzerhof, Hybrid functionals based on a screened Coulomb potential, *J. Chem. Phys.* **118**, 8207 (2003).
- [36] A. A. Mostofi, J. R. Yates, G. Pizzi, Y.-S. Lee, I. Souza, D. Vanderbilt, and N. Marzari, An updated version of wannier90: A tool for obtaining maximally-localised Wannier functions, *Comput. Phys. Commun.* **185**, 2309 (2014).
- [37] H. Schäfer and H. G. Schnering, Metall-metall-bindungen bei niederen halogeniden, oxyden und oxydhalogeniden schwerer Übergangsmetalle thermochemische und strukturelle prinzipien, *Angew. Chem.* **76**, 833 (1964).
- [38] S. N. Magonov, P. Zoennchen, H. Rotter, H. J. Cantow, G. Thiele, J. Ren, and M. H. Whangbo, Scanning tunneling and atomic force microscopy study of layered transition metal halides Nb₃X₈ (X = Cl, Br, I), *J. Am. Chem. Soc.* **115**, 2495 (1993).
- [39] C. M. Pasco, I. El Baggari, E. Bianco, L. F. Kourkoutis, and T. M. McQueen, Tunable magnetic transition to a singlet ground state in a 2D van der Waals layered trimerized Kagomé magnet, *ACS Nano* **13**, 9457 (2019).
- [40] Y. Haraguchi, C. Michioka, M. Ishikawa, Y. Nakano, H. Yamochi, H. Ueda, and K. Yoshimura, Magnetic-nonmagnetic phase transition with interlayer charge disproportionation of Nb₃ trimers in the cluster compound Nb₃Cl₈, *Inorg. Chem.* **56**, 3483 (2017).
- [41] B. J. Kim, B. J. Jeong, S. Oh, S. Chae, K. H. Choi, S. S. Nanda, T. Nasir, S. H. Lee, K.-W. Kim, H. K. Lim, L. Chi, I. J. Choi, M.-K. Hong, D. K. Yi, H. K. Yu, J.-H. Lee, and J.-Y. Choi, Structural and electrical properties of Nb₃I₈ layered crystal, *Phys. Status Solidi RRL* **13**, 1800448 (2019).
- [42] See Supplemental Material at <http://link.aps.org/supplemental/10.1103/PhysRevB.102.035412> for more details on the electronic properties of SL Nb₃X₈.
- [43] J. Jiang, Q. Liang, R. Meng, Q. Yang, C. Tan, X. Sun, and X. Chen, Exploration of new ferromagnetic, semiconducting and biocompatible Nb₃X₈ (X = Cl, Br or I) monolayers with considerable visible and infrared light absorption, *Nanoscale* **9**, 2992 (2017).
- [44] Y. Haraguchi, C. Michioka, M. Imai, H. Ueda, and K. Yoshimura, Spin-liquid behavior in the spin-frustrated Mo₃ cluster magnet Li₂ScMo₃O₈ in contrast to magnetic ordering in isomorphous Li₂InMo₃O₈, *Phys. Rev. B* **92**, 014409 (2015).

- [45] J. Carrasquilla, G. Chen, and R. G. Melko, Tripartite entangled plaquette state in a cluster magnet, *Phys. Rev. B* **96**, 054405 (2017).
- [46] M.-H. Whangbo, H. Xiang, H.-J. Koo, E. E. Gordon, and J. L. Whitten, Electronic and structural factors controlling the spin orientations of magnetic ions, *Inorg. Chem.* **58**, 11854 (2019).
- [47] M.-H. Whangbo, E. E. Gordon, H. Xiang, H.-J. Koo, and C. Lee, Prediction of spin orientations in terms of HOMO-LUMO interactions using spin-orbit coupling as perturbation, *Acc. Chem. Res.* **48**, 3080 (2015).
- [48] E. Tang, J.-W. Mei, and X.-G. Wen, High-temperature fractional quantum Hall states, *Phys. Rev. Lett.* **106**, 236802 (2011).
- [49] L. Z. Zhang, Z. F. Wang, B. Huang, B. Cui, Z. Wang, S. X. Du, H.-J. Gao, and F. Liu, Intrinsic two-dimensional organic topological insulators in metal-dicyanoanthracene lattices, *Nano Lett.* **16**, 2072 (2016).
- [50] D. J. Thouless, M. Kohmoto, M. P. Nightingale, and M. den Nijs, Quantized Hall Conductance in a Two-Dimensional Periodic Potential, *Phys. Rev. Lett.* **49**, 405 (1982).
- [51] T. Cai, S. A. Yang, X. Li, F. Zhang, J. Shi, W. Yao, and Q. Niu, Magnetic control of the valley degree of freedom of massive Dirac fermions with application to transition metal dichalcogenides, *Phys. Rev. B* **88**, 115140 (2013).